Gustavo A. Andreasen[1]
Instituto de Investigaciones Fisicoquímicas Teóricas y Aplicadas (INIFTA), Facultad de Ciencias Exactas, Universidad Nacional de La Plata (UNLP)-Consejo Nacional de Investigaciones Científicas y Técnicas (CONICET), Diagonal 113 y 64, CC. 16, Suc. 4, La Plata 1900, Argentina
e-mail: gandreasen@inifta.unlp.edu.ar

Silvina G. Ramos
Instituto de Investigaciones Fisicoquímicas Teóricas y Aplicadas (INIFTA), Facultad de Ciencias Exactas, Universidad Nacional de La Plata (UNLP)-Consejo Nacional de Investigaciones Científicas y Técnicas (CONICET), Diagonal 113 y 64, CC. 16, Suc. 4, La Plata 1900, Argentina
e-mail: sramos@inifta.unlp.edu.ar

Hernán A. Peretti
Centro Atómico Bariloche-Comisión Nacional de Energía Atómica (CNEA), Av. E. Bustillo 9500, San Carlos de Bariloche, Río Negro 8400, Argentina
e-mail: hernan.americo.peretti@gmail.com

Walter E. Triaca
Instituto de Investigaciones Fisicoquímicas Teóricas y Aplicadas (INIFTA), Facultad de Ciencias Exactas, Universidad Nacional de La Plata (UNLP)-Consejo Nacional de Investigaciones Científicas y Técnicas (CONICET), Diagonal 113 y 64, CC. 16, Suc. 4, La Plata 1900, Argentina
e-mail: walter.triaca@speedy.com.ar

Performance of a Thermally Coupled Hydrogen Storage and Fuel Cell System Under Different Operation Conditions

The performance of a hydrogen storage prototype loaded with AB_5H_6 hydride, whose equilibrium pressure makes it suitable for both feeding a H_2/air proton exchange membrane (PEM) fuel cell and being charged directly from a low-pressure water electrolyzer, interacting thermally with the fuel cell exhaust air, is reported. The nominal 70 L hydrogen storage capacity of the prototype suffices for hydrogen delivery at 0.5 L min^{-1}, which allows a power supply of 50 W for 140 min from the H_2/air fuel cell in the absence of thermal interaction. The storage prototype was characterized by monitoring the internal pressure and the temperatures of the external wall and at the center inside the container at different hydrogen discharge conditions. The responses of the integrated system after either immersing the metal hydride container in air or exposing it to the fuel cell hot exhaust air stream under forced convection were compared. The system shows the best performance when the heat generated at the fuel cell is used to increase the metal hydride container temperature, allowing the operation of the fuel cell at 280 W for 16 min at a high hydrogen flow rate of 4 L min^{-1}. [DOI: 10.1115/1.4035100]

1 Introduction

The use of hydrogen as a highly energetic fuel with pollutant-free exhaust is of increasing interest [1], particularly in applications, such as hybrid electric vehicles [2–3]. The requirements for the use of hydrogen in high-efficiency fuel cells also involve its production from renewable energy sources at low cost, and safe and compact devices for its storage [1,4]. Storing hydrogen from the gaseous phase as metal hydride is a safe and efficient way for energy storage for both stationary and mobile applications [5,6]. Hydride formation and decomposition is a reversible process that involves a large amount of reaction heat. Hence, it is important to consider the thermal transfer conditions from the metal hydride to the environment and vice versa, in order to improve the hydrogen sorption process efficiency [7]. Therefore, the metal hydride container needs to be carefully designed to improve the heat exchange transfer process. The inherent low effective thermal conductivity of the hydride powder combined with the high heat of dehydriding/hydriding reaction makes it necessary to drive heat conveniently in order to reduce the reaction time to practical limits [8,9]. For this purpose, it is possible to increase the effective thermal conductivity by adding a conductive binder, or by using extended surfaces. Considering the latter option, the use of fins oriented perpendicularly to the external surface of the metal hydride container assures a more efficient straight heat flow in the radial direction diminishing thermal gradients, as was demonstrated in an experimental study recently carried out in our laboratory on a cylindrical container, filled with AB_5H_6 hydride, provided with internal and external fins [10].

Numerous investigations related to hydrogen storage devices combined with fuel cells have been performed [11–14]. Some researchers emphasize the importance of using the waste exhaust heat from a H_2/air proton exchange membrane (PEM) fuel cell in a metal hydride container in order to increase the equilibrium pressure of the hydride and hence improve the efficiency of the stored hydrogen recovery [15,16].

[1]Corresponding author.

Manuscript received April 1, 2016; final manuscript received October 26, 2016; published online November 16, 2016. Assoc. Editor: Robert J. Braun.

A new design for a thermally coupled hydrogen storage and fuel cell system, where the heat produced during the H_2/air PEM fuel cell operation is used to enhance the release of hydrogen from the metal hydride container, is presented. The new design involves a vertical arrangement of the hydrogen storage device and the use of the fuel cell exhaust air as the heat transfer fluid instead of water-circulating loops that are used in most of the reported thermally coupled systems [12,16,17], which require additional energy for water pumps, electrovalves, and control systems. The performance of the thermally integrated system under different operation conditions is evaluated. It is worthwhile noting that without thermal interaction, it is not possible to utilize the full hydrogen storage capacity of the prototype due to the cooling of the metal hydride container during hydrogen delivery [17,18].

2 Experimental

2.1 The Hydrogen Storage Device. The hydride-forming material selected to fill the hydrogen storage device is $MmNi_{4.7}Al_{0.3}$, an AB_5-type metal alloy that is a variant of $LaNi_5$, where Mm stands for "mischmetal," a mix of rare earths (56% Ce, 18% La, 13% Nd, 5% Pr, 2% Fe, 2% Y, and 4% other rare earths). The physicochemical equilibrium properties of this hydride-forming AB_5-type metal were determined through pressure-composition isotherm measurements (Fig. 1) in a portable and fully automatic Sievert type equipment. The metal alloy absorbs hydrogen forming AB_5H_6 hydride, which has an equilibrium pressure of 350 kPa at 20 °C that makes it suitable for both feeding a H_2/air PEM fuel cell and being charged directly from a low-pressure water electrolyzer without the need of additional compression.

The metal hydride container used in the present work is similar to the one reported previously [10,19]. It is made of 304 L stainless steel and has internal and external aluminum fins in order to aid heat conduction during the hydrogen sorption process (Fig. 2). The dimensions of the container are: 50 mm outside diameter, 2 mm wall thickness, and 200 mm length. It has an O-ring sealed flange at the top end, a sintered copper filter, a pressure transducer, a shutoff valve, and a 1/4 in National Pipe Thread connector. The internal fins are disks cut out from 0.06 mm thick aluminum foil, which are located inside the container, perpendicularly to its axis, as shown schematically in Fig. 3. They have a central hole that helps their positioning by a centering guide. They are mounted while loading the container with the hydride-forming alloy powder, so that a stack of 60 sandwich-type layers (foil/hydride/foil) of about 2 mm width is built up. In order to allow the passage of hydrogen, the disks have needle puncture type holes with a density of about 15 holes cm^{-2}. The radii of the disks are 2 mm larger than the cylinder internal radius, and a 90 deg fold is applied to this extra portion of radius all around the rim, so that when the disks are inserted inside the container, they make better contact with its internal wall surface. At the same time, the folded rim defines the width of the alloy layers by keeping the distance between consecutive disks. Thus, the internal fins contribute not only to driving heat in the radial direction but also help maintain

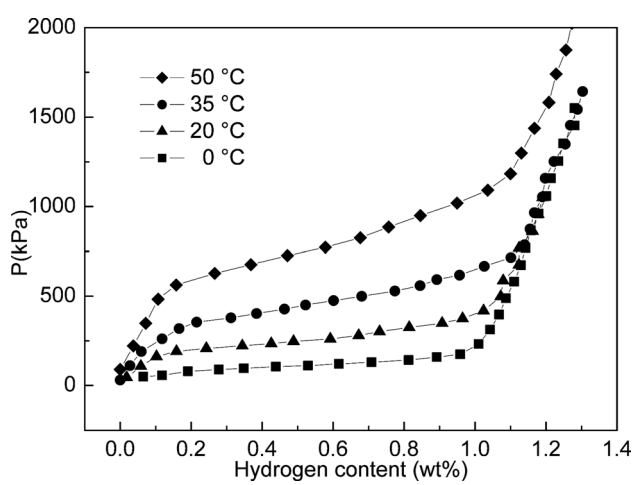

Fig. 1 *P–C* isotherms for $MmNi_{4.7}Al_{0.3}$ alloy

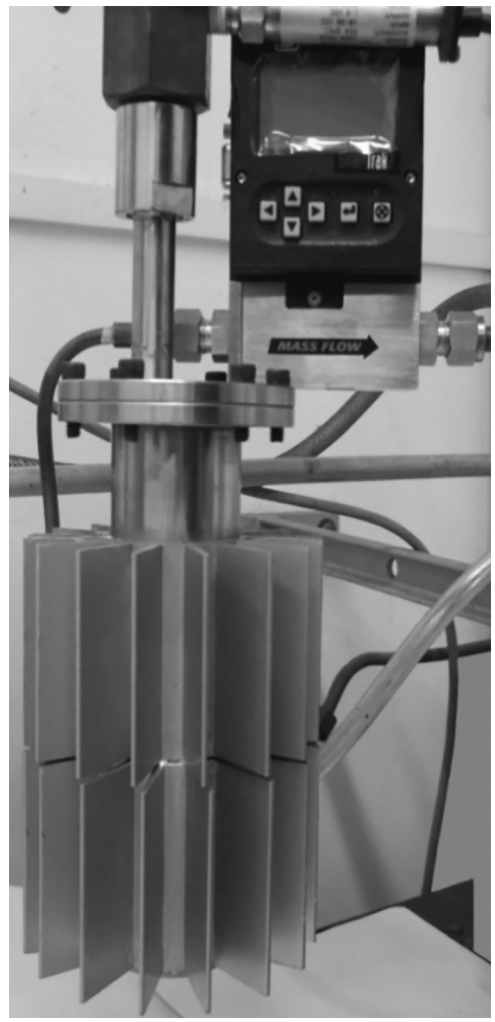

Fig. 2 Metal hydride container

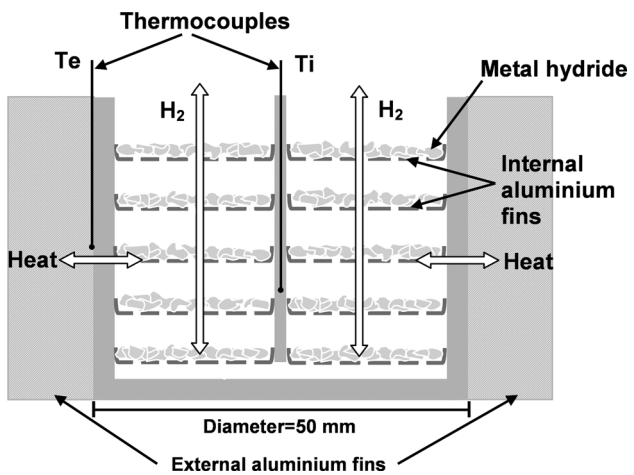

Fig. 3 Scheme of the metal hydride bed. Te = container external wall temperature. Ti = hydride bed temperature.

the metal hydride powder somehow confined to the space between the fins, diminishing powder compaction. The centering guide, made of a copper tube, allows the insertion of a 1/800 stainless steel tube with closed end, welded to the top cover flange, for the measurement of the temperature of the metal hydride at the central axis of the container by means of a thermocouple. On the other hand, 16 external longitudinal fins 30 mm wide and 150 mm long are made from standard heat sinks mechanically attached to the surface of the container (Fig. 2).

The hydrogen storage device was initially loaded with 500 g of hydride-forming metal alloy. After the full hydrogen charge (see Sec. 2.3), the nominal 70 L hydrogen storage capacity of the container (20 °C and 101.3 kPa = 1 atm) suffices for ca. 140 min operation of a 50 W H_2/air fuel cell stack [10,20].

2.2 PEM Fuel Cell Stack. An FCgen®-1020ACS fuel cell stack (ten cells, Ballard Power Systems Inc., Burnaby, Canada) was used (Fig. 4). The H_2/air PEM fuel cell stack is designed to provide stable electrical power while operating over a wide range of operating and environmental conditions. The coolant and oxidant requirements are met with a fan that moves air through the stack. The air is used to cool the stack as well as to provide oxidant for the fuel cell reaction. No external humidification of the air is required. It is designed in a dead-end configuration and for using dry hydrogen, with no external humidification required. The power peak of the stack is approximately 300 W at 5 V.

2.3 Experimental Setup and Measurements. For the experiments, the metal hydride container was connected to the fuel cell stack by a hydrogen-calibrated digital mass flow controller (Sierra Smart-Trak 2 Series 100), and the hydrogen pressure was measured using an Omega PX603 pressure transducer.

A Delta Electronics fan (92 × 92 mm, 12 V–1 A, and maximum air flow of 3.1 $m^3\ min^{-1}$ at 4800 rpm) pushes air through the fuel cell stack providing oxygen for the electrodic reaction and delivering the amount of airflow needed to cool the stack and maintain it at the optimal temperature for a given power. In most situations, the coolant flow requirement far exceeds the oxidant flow demand.

An Agilent electronic load module N3304A, 60 V–60 A was used to get the desired current drain, and the temperatures were measured using type-K thermocouples (Fluke 189).

Experiments consisted of monitoring the time dependence of the hydrogen dynamic pressure [20], which was measured at the outlet of the storage unit, during hydrogen discharges at fixed flow rates and at constant external environment temperature (Ts). At the same time, temperatures at the center of the container loaded with metal hydride (Ti) and at its external wall (Te) were also measured along the hydrogen discharge by using thermocouples.

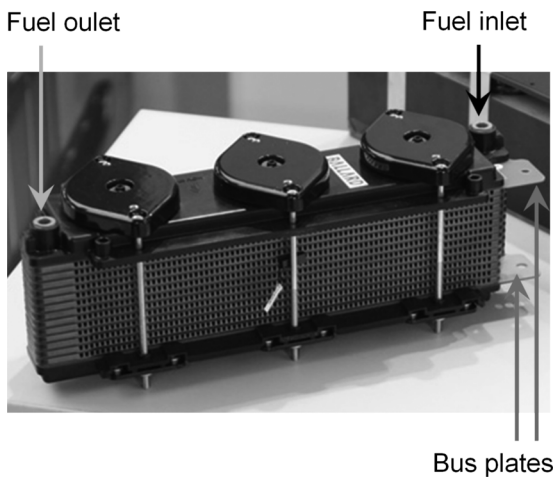

Fig. 4 Fuel cell stack assembly

The hydrogen discharge measurements were performed after a previous hydrogen charge process with high-purity hydrogen (99.999%) at 2500 kPa. The container was considered fully charged when the hydrogen flow stopped and the container recovered its initial room temperature (20 °C), which had risen up due to the exothermic hydrogen absorption reaction.

For the hydrogen discharge runs, a constant flow rate could be established within the range 0.5–5 L min^{-1} (1 L min^{-1} = 4.2 × 10^{-2} moles min^{-1}). The hydrogen flow rate denoted by J is expressed in liters per minute and referred to room conditions (20 °C and 101.3 kPa). Otherwise, concerning the oxidant flow through the fuel cell, the stoichiometric rate is defined as the required airflow to provide the exact number of oxygen molecules to complete the fuel cell reaction for a given current [21]. The oxidant reaction stoichiometry (stoich) is defined as the total airflow divided by the stoichiometric rate [21]. At a room temperature of 20 °C, the cooling airflow requirement exceeds the oxidant stoichiometry requirement, but this does not cause performance loss. According to the fuel cell manufacturer, a stoich of 20 should be used when setting the minimum fan speed during fuel cell startup [21]. It must also be noted that for each power delivered for the fuel cell, the operating temperature was selected according to the manufacturer's recommendations [21].

Hydrogen discharge measurements were carried out under different heat exchange conditions between the metal hydride container and the external environment:

(i) *Natural convection*: The container is exposed to air at room temperature (Ts) without fuel cell thermal interaction (WTI), and this case is denoted as WTI condition.
(ii) *Forced convection*: The fuel cell hot exhaust air stream is driven to the container aluminum fins in order to increase the metal hydride temperature inside the container and hence the dehydriding kinetics and the dynamic equilibrium pressure. This situation is accomplished by means of the air pushed by a fan located upstream the fuel cell (Fig. 5), and this case is called metal hydride container with fuel cell thermal interaction (TI) and denoted as TI condition. The fuel cell exhaust air temperature is similar to the optimal fuel cell temperature (Tc) for a given current delivery, as specified by the fuel cell manufacturer, and the air velocity around the container is estimated to vary between 0.05 and 0.5 m s^{-1}.

In all the cases, the hydride container was in vertical position, according to the design of external fins.

All the hydrogen discharge measurements were stopped according to an adopted cutoff criterion, consisting of preventing the pressure from becoming lower than 107 kPa, which is the minimal fuel cell operating pressure to avoid the entrance of atmospheric gases into the container.

In order to evaluate the hydrogen storage capacity of the container, the hydrogen mass absorbed during the charge process was measured employing the mass flow controller. As a result, both charged and discharged hydrogen mass values were consistent and in agreement with the nominal storage capacity of the container. This also implies that any residual amount of hydrogen remaining in the alloy void spaces after the discharge run is negligible compared to the total amount of desorbed hydrogen.

3 Results and Discussion

3.1 Hydrogen Discharge Rate at 0.5 L min^{-1}. The effect of the fuel cell thermal coupling on the metal hydride container performance was evaluated, and the results were compared with those obtained in the same container without fuel cell thermal interaction. Thus, the metal hydride container was initially tested for a hydrogen desorption flow rate according to its design

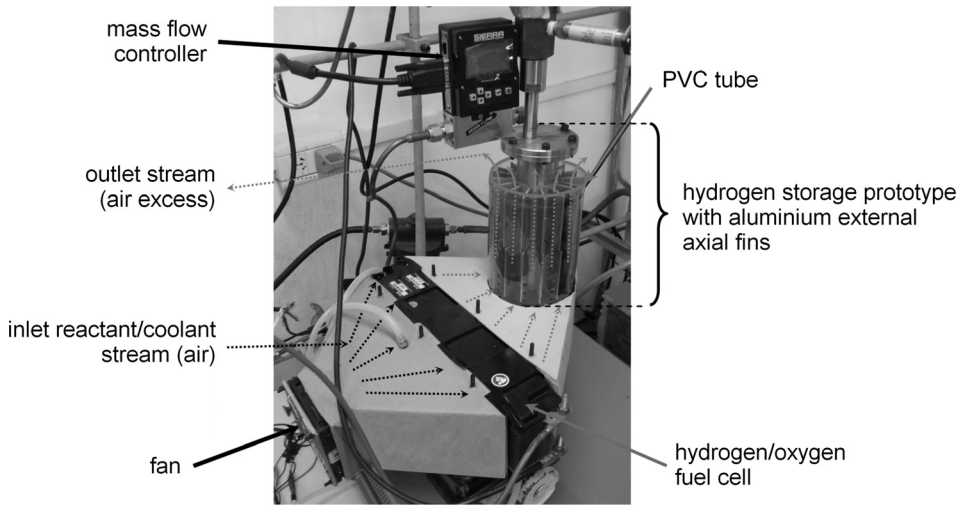

Fig. 5 Hydrogen-based fuel cell and energy storage system under TI condition

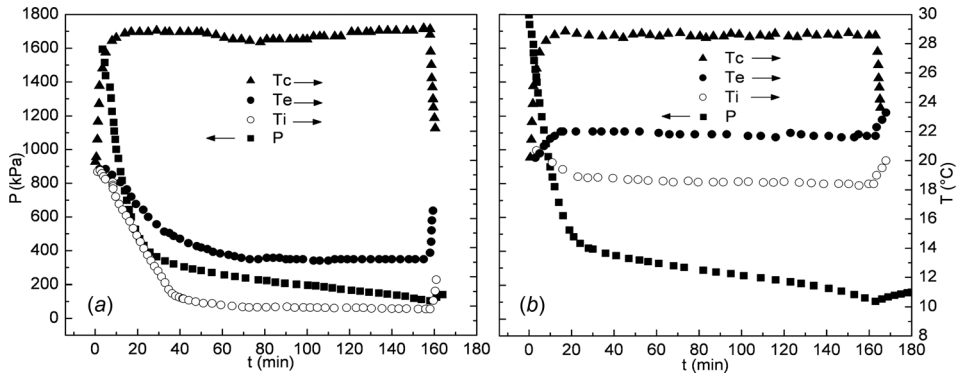

Fig. 6 Fuel cell temperature (Tc), external wall temperature (Te), internal temperature (Ti), and hydrogen pressure (*P*) in the hydride container as a function of time for $J_{H_2} = 0.5\,\mathrm{L\,min^{-1}}$: (*a*) WTI condition and (*b*) TI condition

condition, i.e., $0.5\,\mathrm{L\,min^{-1}}$ in air at room conditions (20 °C and 101.3 kPa). Additional tests were also performed at 1, 2, 4, and $5\,\mathrm{L\,min^{-1}}$ for the sake of characterizing the storage device prototype behavior for heavy-duty conditions.

The plots of the hydrogen dynamic pressure (P) and temperatures of the container (Te and Ti) and the fuel cell (Tc) as a function of time corresponding to discharges at $0.5\,\mathrm{L\,min^{-1}}$ are shown in Fig. 6. The measurements were carried out with the container either in air at Ts = 20 °C (natural convection, WTI condition), Fig. 6(*a*), or exposed to the fuel cell exhaust hot air stream at Tc = 28 °C (forced convection, TI condition), Fig. 6(*b*). The fuel cell temperature corresponds to the optimal temperature recommended by the fuel cell manufacturer for this current delivery, i.e., $i = 6$ A at 7.3 V ($P_w = 44$ W) [21].

The final internal and external temperatures of the container are lower in case (a) than in case (b), but in both cases the same amount of hydrogen is desorbed in spite of a small decrease of the dynamic pressure.

A general feature of the P versus time curves is an abrupt initial pressure drop, corresponding mainly to the release of the compressed hydrogen gas inside the container, until a smooth pressure decrease is attained, which constitutes a "dynamic plateau" due to metal hydride decomposition [20]. This part of the curve is the most affected by the change in the temperature of the metal hydride.

The amount of recovered hydrogen stored as metal hydride can be estimated by calculating the amount of released gas along the dynamic plateau. Thus, considering that the plateau extends from about 20–160 min, the recovered hydrogen flowing at $0.5\,\mathrm{L\,min^{-1}}$ (6.9×10^{-4} g $\mathrm{s^{-1}}$) for 140 min is ca. 70 L for both WTI and TI conditions.

It can be observed that the discharge curves corresponding to both WTI and TI cases almost overlap, practically releasing the same amount of hydrogen.

3.2 Hydrogen Discharge Rate at $2\,\mathrm{L\,min^{-1}}$. The plots of the hydrogen dynamic pressure (P) and temperatures of the metal hydride container (Te and Ti) and the fuel cell (Tc) as a function of time, corresponding to hydrogen discharges at $2\,\mathrm{L\,min^{-1}}$, are shown in Fig. 7. The measurements were carried out with the container either in air at Ts = 20 °C (WTI condition) (Fig. 7(*a*)) or exposed to the fuel cell hot exhaust air stream at 37 °C (TI condition) (Fig. 7(*b*)). The fuel cell temperature is the same in Figs. 7(*a*) and 7(*b*), i.e., Tc = 37 °C, and corresponds to the optimal temperature recommended by the fuel cell manufacturer for this current delivery, i.e., $i = 24$ A at 6.8 V ($P_w = 163$ W).

The final internal and external temperatures of the metal hydride container at the cutoff pressure are approximately 14 °C lower in case (a) than in case (b). The first part of the curves, compressed hydrogen release zone, is similar in all the tests performed, but there is a more pronounced decrease in P and a shortening in the length of the dynamic plateau for the WTI condition. Thus, in case (a) less amount of hydrogen is desorbed because the hydride dynamic plateau reaches the cutoff pressure before all the stored hydrogen is desorbed. The amount of

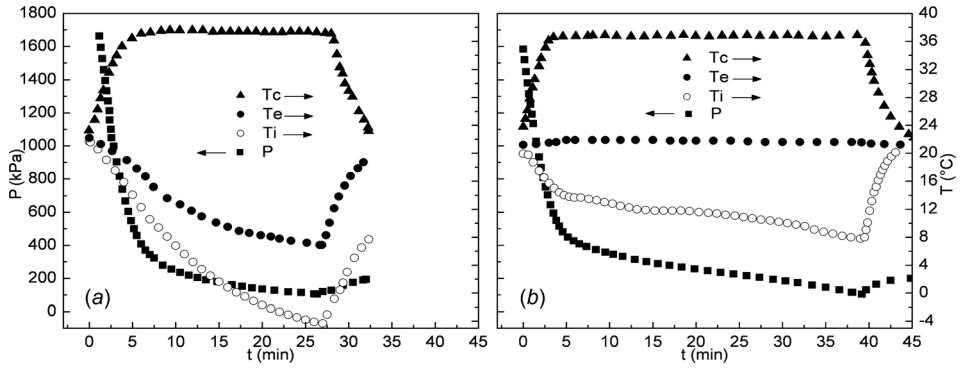

Fig. 7 Fuel cell temperature (Tc), external wall temperature (Te), internal temperature (Ti), and hydrogen pressure (*P*) in the hydride container as a function of time for $J_{H_2} = 2\,\mathrm{L\,min^{-1}}$: (*a*) WTI condition and (*b*) TI condition

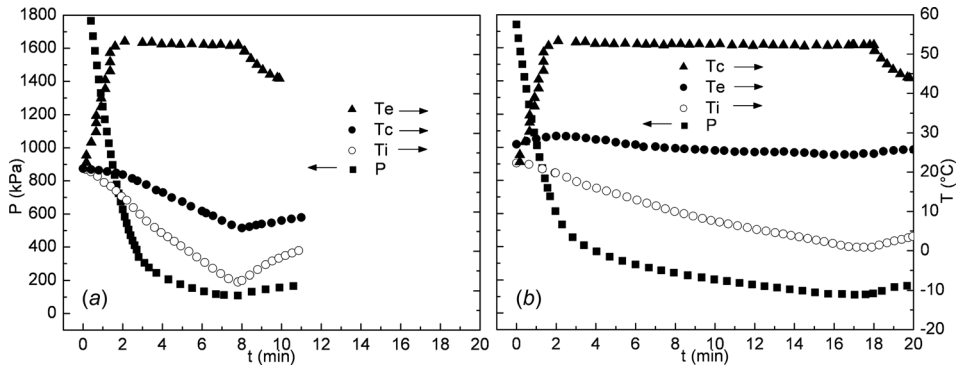

Fig. 8 Fuel cell temperature (Tc), external wall temperature (Te), internal temperature (Ti), and hydrogen pressure (*P*) in the hydride container as a function of time for $J_{H_2} = 4\,\mathrm{L\,min^{-1}}$: (*a*) WTI condition and (*b*) TI condition

recovered hydrogen stored as metal hydride can be estimated from the plateau considering the duration of the hydrogen discharge from 4.5 to 26 min (Fig. 7(*a*)). In this case (WTI condition), the amount of recovered hydrogen flowing at $2\,\mathrm{L\,min^{-1}}$ (2.76×10^{-3} g $\mathrm{s^{-1}}$) for 21.5 min is ca. 43 L. Under TI condition, the plateau extends from 3 to 38 min (Fig. 7(*b*)), reaching a hydrogen recovery of 70 L, i.e., the total amount of stored hydrogen. This implies that hydrogen recovery is 65% larger in case (b) than in case (a) due to a larger heat exchange between the hydride container wall and the forced fuel cell exhaust air at 37 °C. This behavior can be understood in terms of the larger lowering of the metal hydride temperature inside the container during hydrogen desorption in case (a) due to the less efficient heat transfer, giving rise to a faster decrease of the dynamic pressure plateau and hence a sooner arrival at the cutoff pressure (Fig. 7(*a*)).

3.3 Hydrogen Discharge Rate at $4\,\mathrm{L\,min^{-1}}$. The plots of the hydrogen dynamic pressure (P) and temperatures of the container (Te and Ti) and the fuel cell (Tc) as a function of time, corresponding to hydrogen discharges at $4\,\mathrm{L\,min^{-1}}$, are shown in Fig. 8. The measurements were carried out with the metal hydride container either in air at Ts = 20 °C (WTI condition) (Fig. 8(*a*)) or exposed to the fuel cell hot exhaust air stream (Fig. 8(*b*)) at 52 °C (TI condition). The fuel cell temperature is the same in both cases and corresponds to the optimal temperature (Tc = 52 °C) recommended by the fuel cell manufacturer for this current delivery, i.e., $i = 45$ A at 6.2 V ($P_w = 280$ W).

The final internal and external temperatures of the hydride container at the cutoff pressure are approximately 18 °C lower in case (a) than in case (b), so in case (a) less amount of hydrogen is desorbed because the hydride dynamic plateau reaches the cutoff pressure before all the stored hydrogen is desorbed.

As in the above-mentioned cases, the first part of the curves (compressed hydrogen zone) is similar, but again important changes at the dynamic plateau are observed. The change is more pronounced for the WTI case, as expected due to the less heat transfer efficiency through the container wall by natural air convection than by forced air in the case of TI. The amount of recovered hydrogen stored as metal hydride in case (a), WTI condition, flowing at $4\,\mathrm{L\,min^{-1}}$ (5.52×10^{-3} g $\mathrm{s^{-1}}$) for 6 min is ca. 24 L, and in case (b), TI condition, is equal to 62 L. This implies an increase of 160% in the amount of recovered hydrogen due to a larger heat exchange between the hydrogen container and the forced fuel cell exhaust air stream at 52 °C in case (b) than in case (a) under WTI condition.

4 Summary of Results

When the metal hydride container in air at 20 °C delivers hydrogen at $0.5\,\mathrm{L\,min^{-1}}$ under the WTI condition, Ti and Te reach constant values, which indicates that the amount of heat required for the dehydriding process is sufficiently provided by heat transfer from the external environment. Therefore, taking the enthalpy change related to hydride decomposition $\Delta H = -24.8$ kJ $\mathrm{mol_{H_2}^{-1}}$ [22], the heat involved per unit time during the hydrogen discharge at $0.5\,\mathrm{L\,min^{-1}}$ (2.1×10^{-2} mol $\mathrm{min^{-1}}$) is 31.25 kJ $\mathrm{h^{-1}}$ (8.6 W). Under these conditions, the fuel cell delivers 6 A at 7.3 V, i.e., 44 W, and the heat per unit time generated by the irreversibility of the fuel cell reactions reaches 31 W (for a fuel cell efficiency, ε, of 58.6%) [21], while only 8.6 W is required to keep the temperature of the hydrogen storage device constant.

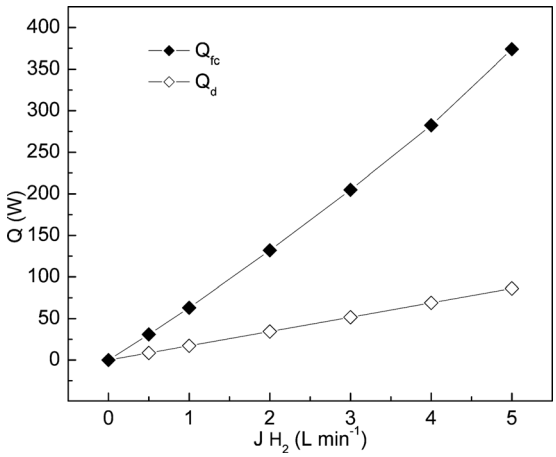

Fig. 9 Dehydriding process heat (Q_d) and heat generated at the fuel cell (Q_{fc}) per unit time versus hydrogen flow rate (J_{H_2})

The heat per unit time required for the dehydriding process (Q_d) and the heat per unit time generated at the fuel cell (Q_{fc}) as a function of hydrogen flow rate are shown in Fig. 9. In the figure, additional data at 1 and 5 L min^{-1} are also plotted. It can be observed that for a hydrogen flow rate of 2 L min^{-1}, the required Q_d value is 34.5 W, while Q_{fc} is 137 W when the fuel cell delivers 24 A at 6.8 V, i.e., 163 W ($\varepsilon = 54.5\%$). Likewise, for a hydrogen flow rate of 4 L min^{-1}, the required Q_d value is 69 W, while Q_{fc} is 283 W when the fuel cell delivers 45 A at 6.2 V, i.e., 280 W ($\varepsilon = 50\%$).

From these results, it follows that the amount of heat generated by the fuel cell at all the hydrogen flow rates is about four times larger than the heat required to recover all the hydrogen stored in the container by the dehydriding process, which is in agreement with data reported elsewhere by using a water-cooled PEM fuel cell [12,16,17] instead of an air-cooled PEM fuel cell as in our case. Therefore, higher operating temperatures of the metal hydride container allow keeping the dynamic pressure over the cutoff value for a longer time, enabling the recovery of all the available stored hydrogen, as can also be inferred from the hydrogen dynamic pressure of the metal hydride container versus released hydrogen mass plot (Fig. 10).

The amount of extra energy obtained from the fuel cell hot exhaust air causes the temperature, and hence the pressure of the metal hydride, to be nearly constant in the 0.5–2 L min^{-1} range on

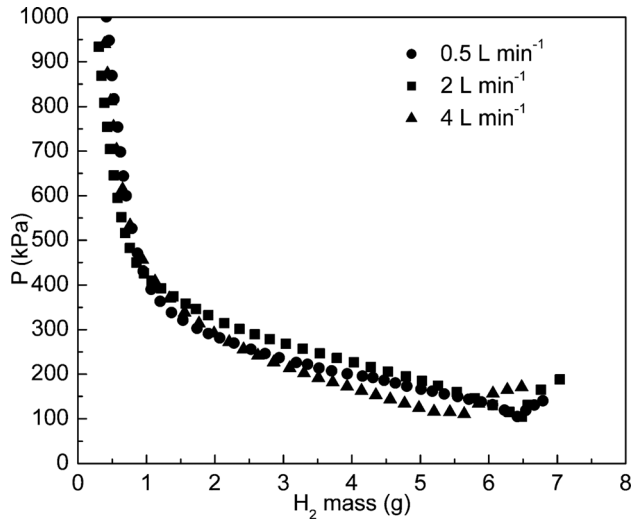

Fig. 10 Hydrogen pressure (P) as a function of released hydrogen mass at different discharge flow rates

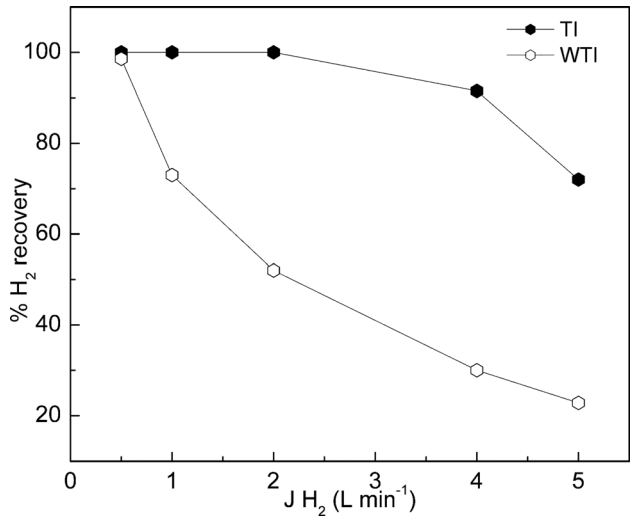

Fig. 11 Recovery efficiency of the hydrogen stored in the container as a function of hydrogen flow rate (J_{H_2}) for TI and WTI conditions

increasing the hydrogen flow rate, avoiding a significant decrease of the dynamic pressure and hence a sooner arrival at the cutoff value, which allows recovering most of the stored hydrogen.

The recovery efficiency of the hydrogen stored in the hydride container as a function of hydrogen flow rate is plotted in Fig. 11. The upper curve shows the hydrogen recovery efficiency when the metal hydride container interacts thermally with the fuel cell (TI condition), while the lower one shows the efficiency for WTI condition.

For hydrogen flow rates in the 0.5–2 L min^{-1} range under the TI condition, the hydrogen recovery efficiency remains practically constant at 100%, while at flow rates higher than 2 L min^{-1} an appreciable decrease is observed. This behavior can be attributed to the fact that at high hydrogen discharge rates, the temperature gradient between the container external wall and the metal hydride at the center of the container increases substantially due to the low effective thermal conductivity of the metal hydride powder, as reflected by the large final (Te–Ti) of ca. 24 °C for a hydrogen flow rate of 4 L min^{-1} under TI condition. Hence, the endothermic effect of the dehydriding reaction begins to prevail and the metal hydride temperature in the container decreases, impeding total hydrogen recovery.

5 Conclusions

A hydrogen storage prototype was built, showing a good performance to recover hydrogen from the stored metal hydride decomposition at the design working conditions, i.e., capable of delivering 70 L of hydrogen at 0.5 L min^{-1} and 20 °C, in order to feed a 50 W hydrogen/air PEM fuel cell for 140 min. This satisfactory behavior is achieved using internal and external finned metal hydride container configurations.

When the metal hydride container is thermally integrated with a H_2/air PEM fuel cell through the fuel cell hot exhaust air, it is possible to operate the system at hydrogen flow rates eight times higher than those for the hydrogen container without fuel cell thermal interaction. Under this condition, most of the stored hydrogen is recovered, without using additional energy for water pumps, electrovalves, and control systems, as required in the case of thermally integrated systems using water-circulating loops.

Higher operating temperatures of the metal hydride container allow keeping the pressure over the cutoff value for a longer time, releasing all the stored hydrogen available.

By adopting this new kind of thermal integration, the operation of the fuel cell is not affected at all, and the fuel cell hot exhaust

air is exploited, favoring the heat transfer through the metal hydride container external wall, which diminishes thermal gradients in the metal hydride bed and leads to a lower decrease of the dynamic pressure. Thus, the total hydrogen stored as metal hydride may be used.

Acknowledgment

This work was financially supported by CONICET, UNLP, and ANPCyT (Argentina). G. Andreasen is a member of the research career of the Comisión de Investigaciones Científicas de la Provincia de Buenos Aires (CIC).

References

[1] Hosseini, S. E., and Wahid, M. A., 2016, "Hydrogen Production From Renewable and Sustainable Energy Resources: Promising Green Energy Carrier for Clean Development," Renewable Sustainable Energy Rev., **57**(1), pp. 850–866.
[2] Eudy, L., Post, M., and Gikakis, C., 2015, "Fuel Cell Buses in U.S. Transit Fleets: Current Status 2015," Technical Report No. NREL/TP-5400-64974.
[3] Davis, S. C., Williams, S. E., Boundy, R. G., and Moore, S., 2016, "2015 Vehicle Technologies Market Report," Technical Report No. ORNL/TM-2016/124.
[4] Carmo, M., Fritz, D. L., Mergel, J., and Stolten, D., 2013, "A Comprehensive Review on PEM Water Electrolysis," Int. J. Hydrogen Energy, **38**(12), pp. 4901–4934.
[5] Satyapal, S., Petrovic, J., Read, C., Thomas, G., and Ordaz, G., 2007, "The U.S. Department of Energy's National Hydrogen Storage Project: Progress Towards Meeting Hydrogen-Powered Vehicle Requirements," Catal. Today, **120**(3–4), pp. 246–256.
[6] Sandrock, G., and Bowman, R. C., Jr., 2003, "Gas-Based Hydride Applications: Recent Progress and Future Needs," J. Alloys Compd., **356–357**(1), pp. 794–799.
[7] Mohan, G., Prakash Maiya, M., and Srinivasa Murthy, S., 2010, "The Performance Simulation of Air-Cooled Hydrogen Storage Device With Plate Fins," Int. J. Low-Carbon Technol., **5**(1), pp. 25–34.
[8] Gadre, S. A., Ebner, A. D., and Ritter, J. A., 2005, "Two Dimensional Model for the Design of Metal Hydride Hydrogen Storage Systems," Adsorption, **11**(1), pp. 871–876.
[9] Gadre, S. A., Ebner, A. D., Al-Muhtaseb, S. A., and Ritter, J. A., 2003, "Practical Modeling of Metal Hydride Hydrogen Storage Systems," Ind. Eng. Chem. Res., **42**(8), pp. 1713–1722.
[10] Andreasen, G., Melnichuk, M., Ramos, S., Corso, H. L., Visintin, A., Triaca, W. E., and Peretti, H. A., 2013, "Hydrogen Desorption From a Hydride Container Under Different Heat Exchange Conditions," Int. J. Hydrogen Energy, **38**(30), pp. 13352–13359.
[11] Delhomme, B., Lanzini, A., Ortigoza-Villalba, G. A., Nachev, S., de Rango, P., Santarelli, M., Marty, P., and Leone, P., 2013, "Coupling and Thermal Integration of a Solid Oxide Fuel Cell With a Magnesium Hydride Tank," Int. J. Hydrogen Energy, **38**(11), pp. 4740–4747.
[12] Khaitan, S. K., and Raju, M., 2012, "Discharge Dynamics of Coupled Fuel Cell and Metal Hydride Hydrogen Storage Bed for Small Wind Hybrid Systems," Int. J. Hydrogen Energy, **37**(3), pp. 2344–2352.
[13] Mellouli, S., Askri, F., Dhaou, H., Jemni, A., and Ben Nasrallah, S., 2010, "Numerical Simulation of Heat and Mass Transfer in Metal Hydride Hydrogen Storage Tanks for Fuel Cell Vehicles," Int. J. Hydrogen Energy, **35**(4), pp. 1693–1705.
[14] MacDonald, B. D., and Rowe, A. M., 2006, "A Thermally Coupled Metal Hydride Hydrogen Storage and Fuel Cell System," J. Power Sources, **161**(1), pp. 346–355.
[15] MacDonald, B. D., and Rowe, A. M., 2006, "Impacts of External Heat Transfer Enhancements on Metal Hydride Storage Tanks," Int. J. Hydrogen Energy, **31**(12), pp. 1721–1731.
[16] Jiang, Z., Dougal, R. A., Liu, S., Gadre, S. A., Ebner, A. D., and Ritter, J. A., 2005, "Simulation of a Thermally Coupled Metal-Hydride Hydrogen Storage and Fuel Cell System," J. Power Sources, **142**(1–2), pp. 92–102.
[17] Førde, T., Eriksen, J., Pettersen, A. G., Vie, P. J. S., and Ulleberg, Ø., 2009, "Thermal Integration of a Metal Hydride Storage Unit and a PEM Fuel Cell Stack," Int. J. Hydrogen Energy, **34**(16), pp. 6730–6739.
[18] Bossi, C., Del Corno, A., Scagliotti, M., and Valli, C., 2007, "Characterisation of a 3 kW PEFC Power System Coupled With a Metal Hydride H_2 Storage," J. Power Sources, **171**(1), pp. 122–129.
[19] Melnichuk, M., Andreasen, G., Corso, H. L., Visintin, A., and Peretti, H. A., 2008, "Study and Characterization of a Metal Hydride Container," Int. J. Hydrogen Energy, **33**(13), pp. 3571–3575.
[20] Goodell, P. D., Sandrock, G. D., and Huston, E. L., 1980, "Kinetic and Dynamic Aspects of Rechargeable Metal Hydrides," J. Less Common Met., **73**(1), pp. 135–142.
[21] Ballard Power Systems, Inc., 2011, "Product Manual and Integration Guide," FCgenVR -1020ACS, MAN5100319-0A, Burnaby, BC, Canada.
[22] Rodríguez, D., 2000, "Estudio y optimización de aleaciones almacenadoras de hidrógeno," Ph.D. thesis, Balseiro Intitute-Universidad Nacional de Cuyo, Bariloche, Argentina.